

PAPER • OPEN ACCESS

Energy offsets within a molecular monolayer: the influence of the molecular environment

To cite this article: M Willenbockel *et al* 2013 *New J. Phys.* **15** 033017

View the [article online](#) for updates and enhancements.

You may also like

- [Growth of ordered molecular layers of PTCDAs on Pb/Si\(111\) surfaces: a scanning tunneling microscopy study](#)
N Nicoara, J Méndez and J M Gómez-Rodríguez
- [Ionic compound mediated rearrangement of 3, 4, 9, 10-perylene tetracarboxylic dianhydride molecules on Ag\(100\) surface](#)
Qinmin Guo, Min Huang, Shuangzan Lu et al.
- [Isotropic thin PTCDAs films on GaN\(0 0 0 1\)](#)
Ch Ahrens, J I Flege, C Jaye et al.

Energy offsets within a molecular monolayer: the influence of the molecular environment

M Willenbockel^{1,2,4}, B Stadtmüller^{1,2}, K Schönauer^{1,2},
F C Bocquet^{1,2}, D Lüftner³, E M Reinisch³, T Ules³, G Koller³,
C Kumpf^{1,2}, S Soubatch^{1,2,4}, P Puschnig³, M G Ramsey³
and F S Tautz^{1,2}

¹ Peter Grünberg Institut (PGI-3), Forschungszentrum Jülich, 52425 Jülich, Germany

² Jülich Aachen Research Alliance (JARA), Fundamentals of Future Information Technology, 52425 Jülich, Germany

³ Institut für Physik, Karl-Franzens-Universität Graz, 8010 Graz, Austria
E-mail: s.subach@fz-juelich.de and m.willenbockel@fz-juelich.de

New Journal of Physics **15** (2013) 033017 (13pp)


Received 14 November 2012

Published 13 March 2013

Online at <http://www.njp.org/>

doi:10.1088/1367-2630/15/3/033017

Abstract. The compressed 3,4,9,10-perylene tetracarboxylic dianhydride (PTCDA) herringbone monolayer structure on Ag(110) is used as a model system to investigate the role of molecule–molecule interactions at metal–organic interfaces. By means of the orbital tomography technique, we can not only distinguish the two inequivalent molecules in the unit cell but also resolve their different energy positions for the highest occupied and the lowest unoccupied molecular orbitals. Density functional theory calculations of a freestanding PTCDA layer identify the electrostatic interaction between neighboring molecules, rather than the adsorption site, as the main reason for the molecular level splitting observed experimentally.

 Online supplementary data available from stacks.iop.org/NJP/15/033017/mmedia

⁴ Authors to whom any correspondence should be addressed.



Content from this work may be used under the terms of the [Creative Commons Attribution 3.0 licence](http://creativecommons.org/licenses/by/3.0/). Any further distribution of this work must maintain attribution to the author(s) and the title of the work, journal citation and DOI.

Contents

1. Introduction	2
2. Experimental details	3
3. Results: geometric structure	3
4. Results: orbital tomography	6
5. Discussion	8
6. Conclusion	12
Acknowledgments	12
References	12

1. Introduction

A fundamental issue in the field of organic–metal interfaces is the influence of molecule–substrate and molecule–molecule interactions on the electronic (and structural) properties of the interface and their relative importance [1–4]. In particular, molecule–molecule interactions are difficult to study quantitatively, because their influence tends to be small. Moreover, in most systems multiple adsorption sites and multiple intermolecular environments coexist, making it difficult to disentangle their influence on the electronic structure of the interface.

Since it has been shown that the angular distribution of photoelectrons can be simply understood in terms of the Fourier transform of the molecular orbitals [5–7], the power of angle resolved photoelectron spectroscopy (ARPES) has been greatly advanced. For example, it has been shown that orbital tomography, i.e. the analysis of the ARPES $I(E_b, k_x, k_y)$ data cube, where I is the photoelectron intensity, E_b is the binding energy and k_x and k_y are the parallel components of the momentum, allows the unambiguous identification of molecular energy levels at organic–metal interfaces even beyond the energy resolution of the spectrometer [7]. In particular, the photoemission (PE) signal from molecules with different in-plane orientation on the surface can be easily distinguished by the characteristic angular photoelectron distribution [8, 9].

In this paper we show that orbital tomography can disentangle the environment-specific electronic structure, i.e. orbital energy level splittings between different molecules in complex structures. Up to now this information was only available from cryogenic scanning tunneling microscopy/spectroscopy (STM/STS) [1, 3, 4, 10–12]. We demonstrate the capability of orbital tomography using the environment-specific electronic structure of the model system 3,4,9,10-perylene tetracarboxylic dianhydride (PTCDA) adsorbed on Ag(110) as an example. This provides an excellent test system because, depending on preparation, either brickwall (BW) or herringbone (HB) monolayers can be formed [9, 13, 14]. In the BW monolayer, all molecules are adsorbed perpendicular to the Ag rows and are identical with respect to their environment, while the HB monolayer has molecules both parallel and perpendicular to the Ag rows which, moreover, differ in their molecular environment and thus intermolecular interactions.

A tomographic analysis of the ARPES reveals an energy level offset between $[001]$ and $[1\bar{1}0]$ oriented molecules for both the emissions from the highest occupied molecular orbitals (HOMO) and those from the lowest unoccupied molecular orbitals (LUMO), the latter being

filled through charge transfer from the metal substrate [15]. In order to reveal the origin of the observed level splittings, we have performed density functional theory (DFT) calculations for freestanding PTCDA layers. The computed HOMO and LUMO splittings are found to be in excellent agreement with the values derived from ARPES experiments and are explained by constant energy level offsets arising from the distinct electrostatic environments of the two inequivalent molecules present in the HB structure.

2. Experimental details

All experiments were carried out at room temperature under ultra-high vacuum conditions with a base pressure of $P < 2 \times 10^{-9}$ mbar. The sample was cleaned by subsequent cycles of Ar⁺ sputtering and annealing up to 800 K. PTCDA molecules were evaporated from a Knudsen cell, while the sample was held at room temperature. Low-energy electron diffraction (LEED) experiments were carried out with a multi-channel plate LEED, using typical beam currents of 1 nA to prevent the molecular film from being damaged by the electron beam.

In our tomographic ARPES experiments, the samples were illuminated with 35 eV photons under an incident angle of $\alpha = 40^\circ$ with respect to the surface normal (BESSY II storage ring, beamline U125/2-SGM). The photoelectrons were recorded with a toroidal electron analyzer. This analyzer allows the simultaneous detection of photoelectrons emitted with polar angles between $\pm 80^\circ$, with kinetic energy differences up to 2 eV and without any change of the incident light polarization. To collect photoelectrons in the full hemisphere above the sample surface, the sample was rotated around its surface normal in steps of 1° . For more details of the toroidal analyzer see [16]. Converting the polar and azimuthal photoelectron take-off angles into parallel momenta (k_x, k_y) [7], we obtain a three-dimensional data cube of the PE signal $I(E_b, k_x, k_y)$ (see the supplementary material, available from stacks.iop.org/NJP/15/033017/mmedia). Taking cross-sections of this data cube at fixed binding energies E_b , constant binding energy momentum space maps (CBE maps) were produced.

The real space electron distributions of the freestanding PTCDA molecule were computed on the level of the generalized gradient approximation (GGA) [17] by ABINIT [18] (cf [7] for details).

The calculations of the freestanding layer were performed with the VASP code [19, 20]. The all-electron potentials were replaced by PAW potentials [21] with a cut-off energy for the plane wave basis set of 500 eV. We used a Gamma centered k -point grid of $6 \times 6 \times 1$ along reciprocal lattice vectors and applied a super-cell approach with a distance of 20 Å between two PTCDA layers to avoid interaction between them. Exchange-correlation effects were treated within the GGA, van der Waals forces were included as semi-empirical dispersion correction according to Grimme [22].

3. Results: geometric structure

Despite being much studied, there has been some confusion in the literature about the PTCDA structures on Ag(110) which has recently been partially corrected [9]. As our calculations have found significant differences in the intermolecular interactions for the various structures that have been reported, it was necessary to repeat and reaccess the LEED investigations.

Upon adsorption on Ag(110) at room temperature, PTCDA molecules form islands by arranging themselves in the BW structure until the surface is completely covered [13, 23, 24].

It consists of parallel oriented molecules aligned with their long axes along the [001] direction of Ag(110) (figures 1(a) and (b)) and is well studied by means of LEED [13, 23], STM [13, 23–25], normal incidence x-ray standing waves [26], ultraviolet photoelectron spectroscopy [9, 15, 27] and orbital tomography [7].

When depositing additional molecules on the BW monolayer, a new pattern appears in LEED, in coexistence with the BW monolayer pattern. Seidel *et al* [14] identified the correct superstructure matrix of this structure from LEED measurements. However, they erroneously assigned this superstructure to a new monolayer structure. Rather, it was shown recently that the new LEED pattern is the signal of an HB layer formed on top of the BW monolayer, i.e. it belongs to a bilayer structure [9]. This interpretation is in agreement with earlier STM results [25]. Figures 1(c) and (d) show a LEED image of the HB-on-BW bilayer, together with the superstructure matrix found in [14] and the corresponding structural model of the upper layer.

We note here that the authors of [9] have incorrectly identified the LEED image of figure 1(c) with the LEED image of the HB *monolayer* which is displayed in figure 1(e). However, there are obvious differences between the two images: while the diffraction pattern of the bilayer has a fourfold rotational symmetry, the HB monolayer exhibits twofold symmetry only.

If the HB-on-BW bilayer or an even thicker film of PTCDA/Ag(110) is annealed to 550 K, an HB monolayer is formed and excess molecules are desorbed [14]. Since this HB monolayer is denser than the BW monolayer, it is often referred to as the ‘compressed monolayer’. The authors of [14] have given an incorrect superstructure matrix for this phase, because the silver substrate directions were confounded⁵. The correct matrix for the compressed monolayer was given by Wießner *et al* [9]. Figures 1(e) and (f) display the LEED pattern, the superstructure matrix and the structure model of the HB monolayer. STM experiments revealed that it consists of two molecules per unit cell, one (molecule A) oriented along the [100] direction (the same orientation as the molecules in the BW phase) and the other (molecule B) along the [1 $\bar{1}$ 0] direction as shown in figures 1(e) and (f) [14]. We note here that molecules A and B are distinguishable not only because of their different orientations with respect to the substrate, but also because of their different positions relative to their neighbors. This is a consequence of the non-orthogonality of the two superstructure unit cell vectors with $\alpha = 91.1^\circ$.

An alternative way to prepare the PTCDA HB monolayer on Ag(110) is the deposition of a submonolayer amount of PTCDA onto one layer of pentacene on Ag(110). Pentacene acts as a surfactant for the preparation of the PTCDA HB monolayer. PTCDA molecules displace pentacene molecules from the metal surface, thereby forming the HB monolayer which is covered by a pentacene layer (floating surfactant). Annealing this PTCDA/pentacene bilayer to 500 K, pentacene desorbs, leaving behind PTCDA in the HB monolayer structure. In this case, the restriction of the available surface area apparently causes PTCDA to condense in the HB structure rather than in the BW structure that forms on clean Ag(110) surfaces. Remarkably, the thus prepared layer does not relax into the BW structure once this spatial restriction is lifted.

The HB monolayer fulfills two conditions which make it an ideal object on which the influence of intermolecular interactions on the electronic properties of the molecules can be investigated by orbital tomography. Firstly, because the two molecules in the unit cell, which

⁵ Because of the fourfold symmetry of its LEED pattern the incorrect assignment of substrate crystal directions does not affect the indexing of the bilayer spots. We note that the LEED result which is reported in [15] to represent a picture of the BW phase is showing the bilayer structure instead.

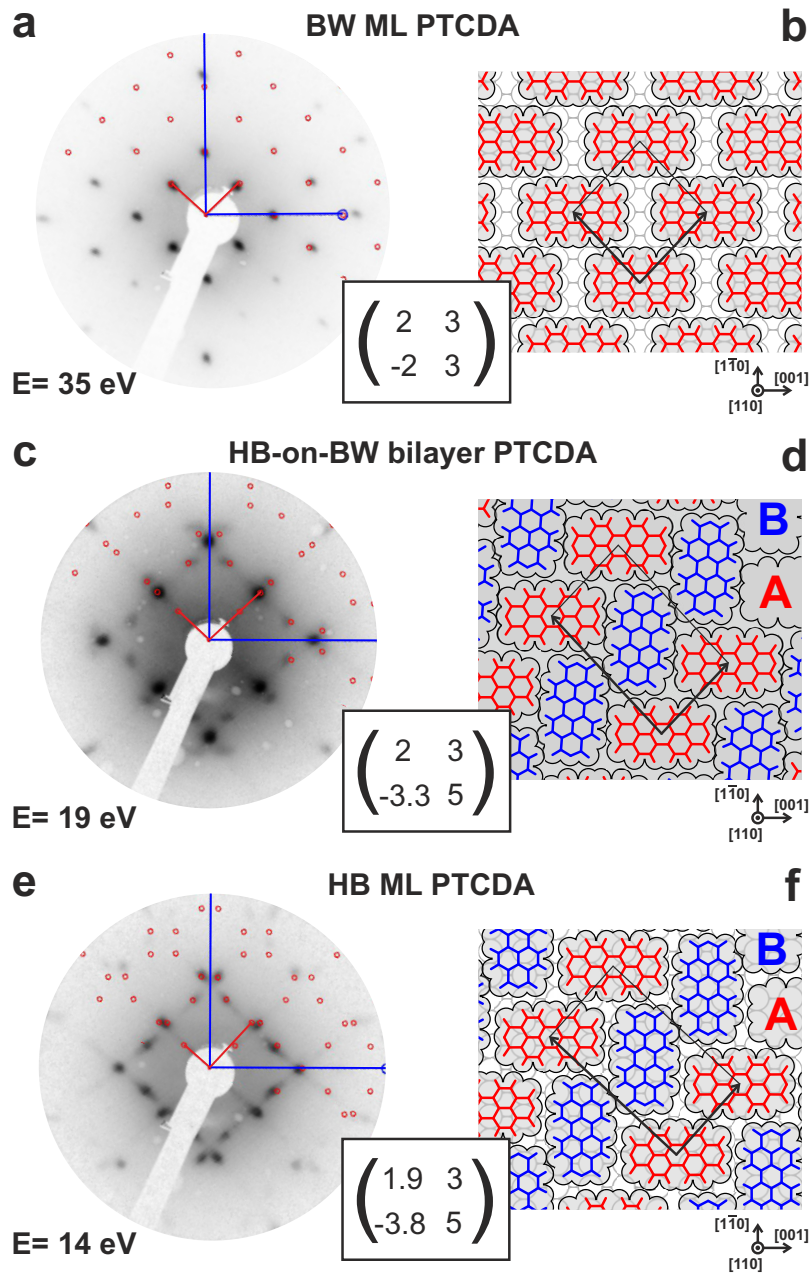


Figure 1. LEED patterns and structure models of the PTCDA/Ag(110) interface with their corresponding superstructure matrices. (a), (b) Brickwall (BW) monolayer, (c), (d) herringbone on brickwall (HB-on-BW) bilayer and (e), (f) herringbone (HB) monolayer (compressed monolayer). One half of each LEED pattern is overlaid by a pattern of calculated spot positions. Blue lines in the LEED image indicate the substrate directions and red lines indicate the reciprocal space unit cell. Black arrows in the structure models indicate the real space unit cell. The two differently oriented molecules in the HB phase unit cells are marked as A (red) and B (blue).

are in different molecular environments, also have different in-plane (azimuthal) orientations, an unambiguous assignment of spectral features to either of the two molecules is possible. Secondly, since the HB monolayer is incommensurate, the influence of the adsorption site on the electronic structure of either of the two distinct types of molecules is averaged out, because in the ARPES experiment we integrate over an essentially infinite number of sites.

4. Results: orbital tomography

In figures 2(a) and (b) two experimental CBE maps (left half of the polar diagrams) of the BW monolayer are shown together with the calculated electron distributions (right half of the polar diagrams). These CBE maps at 1.96 and 0.76 eV binding energy (E_b) reveal the angular PE patterns of the HOMO (a) and LUMO (b) of a single PTCDA molecule and hence match the results of previous studies [7, 15, 27].

CBE maps acquired under the same conditions from the HB monolayer reveal more complex patterns (figure 2(c) for the HOMO and figure 2(d) for the LUMO). Nonetheless, on simple inspection of these CBE maps, one finds that both HOMO and LUMO maps of the HB monolayer consist of a superposition of two identical patterns that are rotated by 90° with respect to each other [9]. This agrees with the arrangement of molecules in the unit cell of the HB monolayer: the unit cell contains two types of molecules (A and B) that are oriented perpendicular to each other (figure 1(f)) [14]. Clearly, molecules of each type give rise to independent but identical anisotropic photoelectron distributions, and the analyzer detects the summed PE intensity. It is also clearly apparent from the data that the intensity contributions of the two orientations at a given energy are not equal. This is because both the HOMO and LUMO PE intensities $I_i(E_b)$ emerging from molecules A and B have different energy dependences, where $i = A, B$ (see the supplementary material, available from stacks.iop.org/NJP/15/033017/mmedia).

To access the energy-dependent photoelectron contributions of the corresponding molecular orbitals separately for the A and B molecules of the HB monolayer, we employ in a first step the k -space deconvolution method proposed in [7]. To this end, theoretical PE momentum maps $\phi_i(k_x, k_y)$ of a free PTCDA molecule were calculated (cf figures 2(a) and (b)) and the corresponding $I(E_b, k_x, k_y)$ data sets were fitted with two identical but 90° -rotated $\phi_i(k_x, k_y)$ patterns for the HOMO and LUMO regions separately, by minimizing the function

$$\chi^2 = \int \int dk_x dk_y \left[I(k_x, k_y, E_b) - \sum_{i=A,B} a_i(E_b) \phi_i(k_x, k_y) \right]^2.$$

The fitting parameters $a_i(E_b)$ represent the projected densities of states (PDOS) for the corresponding orbitals of molecules oriented along $[001]$ (A + BW) and along $[1\bar{1}0]$ (B), if the peaks do not cross the Fermi edge. In the present case, this boundary condition is fulfilled and the resulting PDOS are shown in figure 3(a). Note, however, that as a result of the fitting described so far, we cannot distinguish between $[001]$ oriented molecules in the HB monolayer (A molecules) and molecules in the BW monolayer which may still be present. Therefore, we have labeled the corresponding components in figure 3(a) as A + BW.

It can be seen in figure 3(a) that the A + BW peaks have a higher integrated signal than the corresponding B peaks. This indicates the existence of the BW monolayer as a minority phase on the surface. To extract the relative amount of this minority phase, we employ two

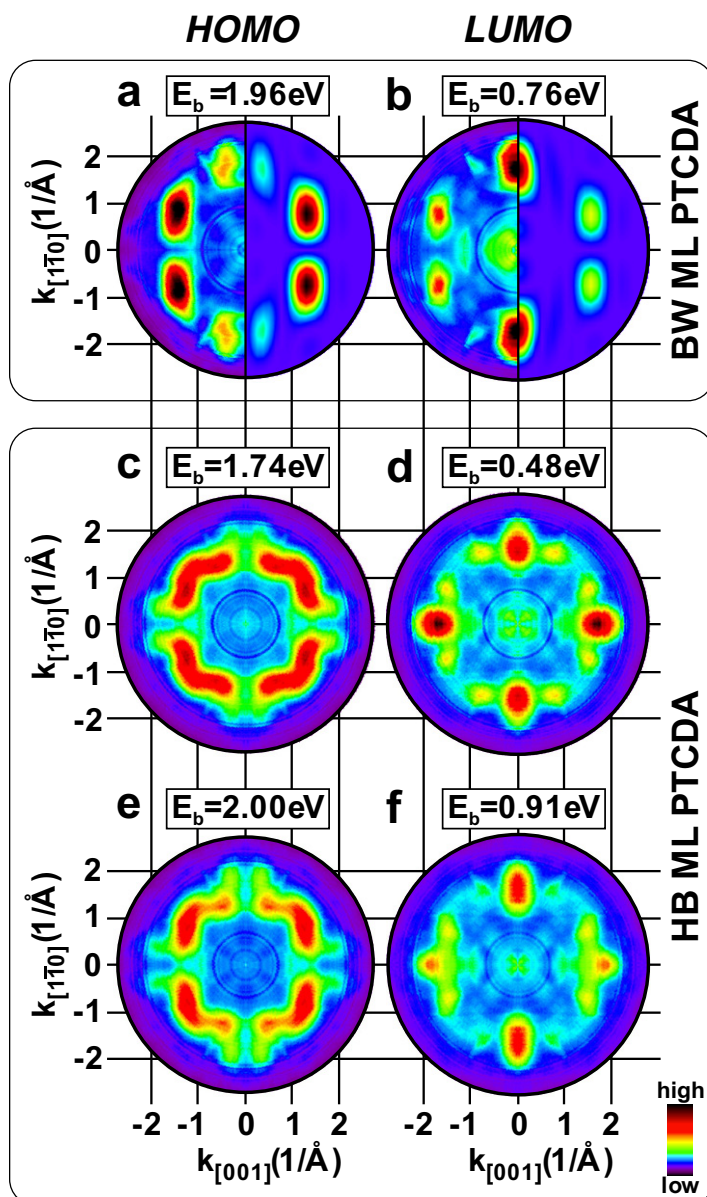


Figure 2. (a), (b) CBE maps of the HOMO (a) and LUMO (b) of the BW monolayer of PTCDA/Ag(110). The right half of each map shows theoretical calculations of the electron distribution in k -space calculated for gas phase molecules. (c), (f) CBE maps of the HOMO (c, e) and LUMO (d, f) of the HB monolayer of PTCDA/Ag(110) at different binding energies. Maps in (c)–(f) are generated from data recorded over an azimuthal angle range of 180° and symmetrized. The colour scale is in arbitrary units.

facts. Firstly, the PDOS of B molecules in figure 3(a) can only arise from the HB monolayer. Secondly, the ratio of A and B molecules in the HB monolayer is known (1:1). Hence, we obtain a minority contribution of less than 20% for the BW monolayer on the surface (from the analysis of the HOMO peaks). Since we know the binding energies of the LUMO (0.75 eV) and HOMO (1.93 eV) in the BW monolayer from our measurements on the pure BW monolayer as well as

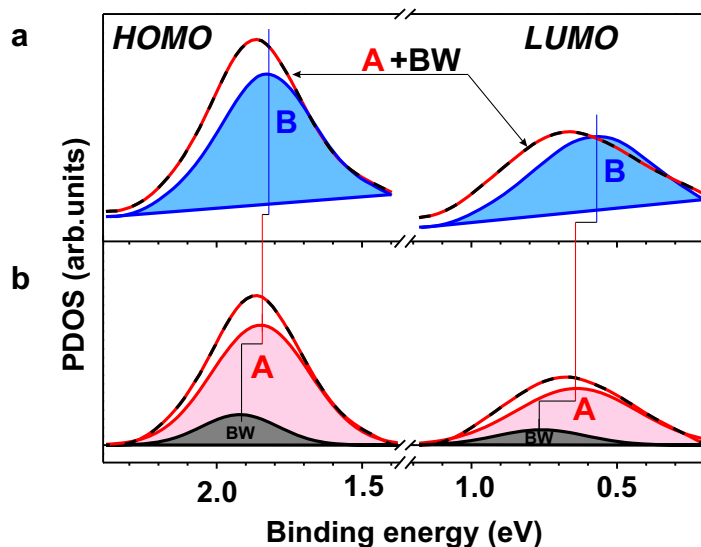


Figure 3. (a) Results for the projected density of states of the HOMO and LUMO extracted from orbital tomography (see text) of the HB monolayer of PTCDA/Ag(110). Two contributions can be identified: the intensity from the B molecules (B, blue) and the joint intensity from the HB A and a minority of BW molecules (A + BW, dashed red/black). (b) Results of the fitting of the joint A + BW contribution (dashed red/black) from panel (a). The BW intensity is shown in black and the HB A molecule intensity in red. A linear background is subtracted for the fitting.

Table 1. Binding energies (BE) and FWHM of the resulting peaks (figure 3) from the orbital tomography and fit procedure (see text) for the molecules in the HB monolayer and the minority BW species. Values marked with an asterisk are fixed in the second step of the fitting procedure and are taken from an experiment with pure BW PTCDA/Ag(110).

	BW _{HOMO}	A _{HOMO}	B _{HOMO}	BW _{LUMO}	A _{LUMO}	B _{LUMO}
BE (eV)	1.93*	1.85	1.83	0.75*	0.64	0.59
FWHM (eV)	0.31	0.39	0.39	0.36	0.49	0.45

from previous experiments [7], we are finally able to separate the A + BW peaks in figure 3(a) into the contributions of BW molecules and A molecules in the HB monolayer, by fitting the A + BW signal by two Gaussian peaks after the subtraction of a linear background. The results are shown in figure 3(b). All the resulting peak positions and full-widths at half-maximum (FWHM) are summarized in table 1.

5. Discussion

From the data in table 1, the following trends can be recognized: (i) HOMO and LUMO levels of molecules in the HB monolayer have significantly smaller binding energies (by at least

80 meV for the HOMO and 110 meV for the LUMO) than molecules in the BW monolayer. (ii) HOMO and LUMO peaks of molecules in the HB monolayer have a larger FWHM than their counterparts in the BW monolayer. (iii) Both in the BW monolayer and in the HB monolayer the LUMO peak is broader than the HOMO peak. This is found for A and B molecules, and is similar to the situation found for PTCDA/Ag(111) [8, 10, 28]. (iv) Finally, within the HB monolayer HOMO and LUMO peaks of molecule A have larger binding energies E_b compared to molecule B, by 20 meV (HOMO) and 50 meV (LUMO).

We now compare the orbital energies of BW and A molecules. Although both molecules are oriented parallel to the [001] direction of Ag, they have different HOMO and LUMO binding energies. The difference amounts to 80 meV for the HOMO and 110 meV for the LUMO. The fact that the BW structure is commensurate and all its molecules are therefore in identical adsorption sites, while the HB monolayer structure is incommensurate, explains that both HOMO and LUMO peaks of the BW phase are sharper (smaller FWHM) than their counterparts in the HB monolayer phase. Another effect which may contribute to the broadening of the peaks in the HB monolayer is the dispersion, which will be discussed later.

However, it is *a priori* not clear whether the difference in peak energies of the HB monolayer can also be explained solely on the basis of the loss of commensurability. Another, possibly even more important reason for this shift may be the difference in intermolecular interactions in the two phases, because the local environment around an A molecule in the HB monolayer differs from that of a molecule in the BW monolayer. This explanation would be in agreement with the results of Kilian *et al* [2], who have compared the LUMO position of single PTCDA molecules adsorbed on Ag(111) and PTCDA molecules in the disordered low-temperature phase on Ag(111) and reported a strong influence of the local molecular environment on the LUMO level, even if the situation regarding the orientation was comparable.

To check whether the binding energy differences between HOMO and LUMO of A and B molecules can indeed be traced back to differences in the respective molecular environments, we have carried out a DFT calculation for a freestanding PTCDA layer in the HB monolayer structure. The results of this calculation are displayed in figures 4(a) and (b). In figure 4(a) we indeed see that A and B molecules have different HOMO and LUMO binding energies. In the case of the HOMO the calculated split amounts to 36 meV, while for the LUMO a split of 41 meV is predicted. Both the sizes of the splittings and their signs (A-HOMO and A-LUMO have larger binding energies than their B counterparts) are in agreement with our experimental findings from orbital tomography. Since the substrate is not considered in the calculation and hence there is no difference in orientation of A and B molecules relative to an external reference direction, and since the effect of the adsorption site in the experiment is expected to be averaged out by the fact that the layer is incommensurate, this agreement between theory and experiment strongly suggests that differences in the molecular environment contribute decisively to the observed binding energy shifts between A and B molecules in the HB monolayer, as well as between the HB and BW monolayers.

Since, as discussed above, the HB-on-BW bilayer structure of figure 1(d) was in the literature mistaken for a second possible single monolayer structure, we also calculated this HB structure as a freestanding monolayer. The result is shown in figures 4(c) and (d). One finds a very large offset of the energy levels for molecules A and B (485 meV for the HOMO). We do not observe such a large offset in our deconvoluted data. This confirms that our sample indeed consisted of the HB monolayer and not of the HB-on-BW bilayer, which has a very similar LEED pattern (figures 1(c) and (e)).

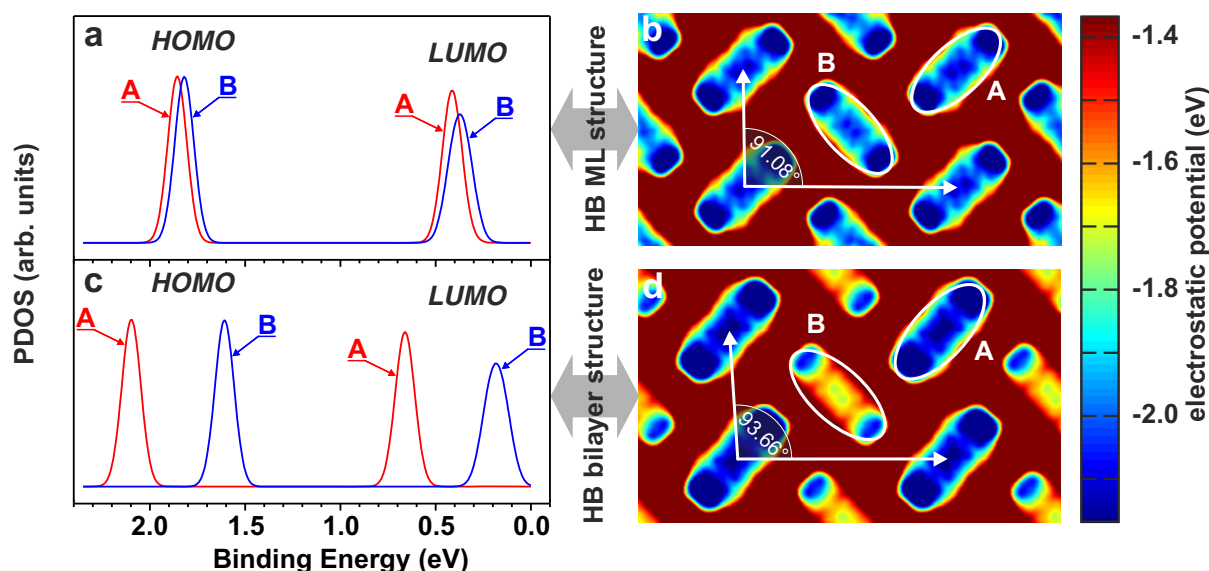


Figure 4. Results of the calculation of the freestanding PTCDA HB monolayer (figure 1(f)) and the freestanding upper layer of the HB-on-BW bilayer (figure 1(d)). (a), (c) Calculated HOMO and LUMO positions of the two inequivalent molecules A (red) and B (blue) with a Gaussian broadening of 50 meV of the HB monolayer (a) and the upper layer of the HB-on-BW bilayer (c). The binding energy of the HB monolayer B-HOMO is aligned with the experiment. (b), (d) Electrostatic potential maps in the plane 1 Å above the calculated layer of the HB monolayer (b) and the upper layer of the HB-on-BW bilayer (d). The regions which were taken into account to calculate an average potential value for molecules A and B are indicated by white ellipses. The unit cell vectors are represented by white arrows.

We note that in the calculation the LUMO of the B molecule is substantially broader than the other three orbitals. This can be traced back to a larger in-plane intermolecular dispersion (due to a larger orbital overlap between neighboring molecules), which yields a band width of 80 meV (compared to 30 meV for the A-LUMO and less than 30 meV for the HOMO of A and B molecules). However, for the freestanding layer one can effectively speak of separate emissions from molecules A and B as the LUMO bands do not cross and effectively there is no hybridization of the orbitals of A and B (see the supplementary material, available from stacks.iop.org/NJP/15/033017/mmedia). In the experiment the LUMO of the B molecule is not significantly broadened with respect to the LUMO of the A molecule. This may be a consequence of the limited analyzer resolution. Moreover, we do not observe any signs of dispersion in our experimental data, i.e. the k -patterns of A and B molecules do not change for different energy slices. This again may be a consequence of limited analyzer resolution.

Finally, we want to address the question of how the molecular environment influences the orbital binding energies. Figures 4(b) and (d) show maps of the local electrostatic potentials of the freestanding layers, with submolecular resolution. The sign of the potential is chosen such that it gives the potential energy of a negative test charge relative to the vacuum level. A potential of -1.0 V means that the work required to remove an electron from this place

to infinity is 1 eV. For both layers the potential distributions for A and B molecules are not identical. On average, A molecules have a more negative potential than B molecules (-1.945 versus -1.891 V) in case of the HB monolayer. This means that on average it costs 54 meV more energy to remove electrons from A molecules than from B molecules. In other words, the apparent binding energy of equivalent electrons is larger by 54 meV in A molecules than in B molecules. For the HB bilayer structure this discrepancy between A molecules (-2.091 V) and B molecules (-1.630 V) is even larger and results in a difference of 461 meV. The fact that the binding energy shifts of the electronic levels are of similar sizes as the potential differences shows that these potential differences are the dominant origin of the observed binding energy offsets between molecules A and B. We note, however, that the HOMO and LUMO levels shift by different amounts when comparing A and B molecules. This is a consequence of the different spatial distributions of the two orbitals; the potential energy map in figure 4(b) is therefore sampled differently for the two orbitals.

Of course, one expects the metal surface to screen the electrostatic fields of the freestanding layer. A DFT calculation of the HB monolayer on the Ag(110) substrate would therefore be desirable. Unfortunately, a direct calculation of the incommensurate HB monolayer on Ag(110) is not possible due to the prohibitively large unit cell, containing at least six PTCDA molecules. The only realistic possibility in the framework of a full DFT calculation to gauge the influence of the metal on the energy offsets between molecules within an HB layer is the calculation of the HB monolayer on the Ag(111) surface, because this structure is commensurate. Such a calculation has been carried out by Rohlfiing *et al* [28]. We have repeated this calculation and obtain essentially identical results. There is, however, a problem with this calculation: while the calculation for the freestanding layer in the geometry of the HB monolayer on Ag(111) yields an energy offset between A and B molecules that is in essential agreement with experimental results, i.e. the binding energies of HOMO and LUMO of B molecules are larger than the corresponding binding energies of A molecules, the screening by the metal leads to a reversal of the order of A and B orbitals: now the HOMO of the A molecule has a larger binding energy than that of the B molecule [28] (we note here that the designation of molecules as A and B on the two surfaces Ag(111) and Ag(110) is arbitrary, and for Ag(111) we follow the convention of Rohlfiing *et al* [28]). While this confirms the influence of the metal, it also shows that DFT is currently unable to predict this influence correctly. Rohlfiing *et al* observe as much and conclude that energy offsets within molecular layers are extremely subtle and may well constitute the limit of the reliability of the calculations, because they may depend on the specifications of the DFT calculation (code, pseudopotential, basis set and exchange correlation functional) and may be subject to many-body effects beyond the present theory [28]. An improved theoretical methodology may clarify the situation in the future.

Nevertheless, to estimate the influence of the screening in the present case of HB layers on Ag(110) semi-quantitatively, we employed an electrostatic model based on the electrostatic potentials calculated for the freestanding layer (figure 4(b)), in which the presence of the metal is taken into account by a simple image potential due to the metallic substrate with a spatial distribution corresponding to the orbital. Since the HB monolayer structure on Ag(110) is incommensurate and one hence does not expect a site-specific screening to show up in the experimental spectra, with the consequence that the effect of screening on the measured orbital energies of A and B molecules is expected to be uniform (except for directional effects), this approximation may not be too bad. Assuming an effective image plane position of 0.5 \AA above the topmost Ag-layer, a rough estimate taken from a comparison with Al from table I

of Garcia–Lastra *et al* [29], the image fields lead to a reduction of the level offsets by roughly 30%. This slightly worsens the agreement of the predicted with the measured energy offsets, but nevertheless suggests the major cause of the energy offsets to be of intermolecular electrostatic origin.

6. Conclusion

We can thus conclude that the offsets observed in the experiment between the orbital binding energies of A and B molecules are very similar to the electrostatic potential difference between A and B molecules. This electrostatic potential difference is a consequence of the molecular quadrupole moments and their associated electric fields. Because of the shape of the HB monolayer unit cell, the sum of all quadrupole fields at the sites of the A molecules is different from that at the sites of the B molecules. For PTCDA/Ag(111) it has also been shown that orbital energy offsets are related to intermolecular interactions [28]. It is remarkable that for both Ag(110) (this work) and Ag(111) [28] the calculations of the freestanding layer lead to an essentially correct prediction, both with regard to the size and the sign of the binding energy offsets between A and B molecules. This leads to the final result that, at least in the case of PTCDA on Ag surfaces, intermolecular interactions contribute decisively to the energy level offsets that are observed within the molecular layer, while the influence of the molecule–substrate interaction appears to be secondary and—as the experiment reveals—does not change the sign of the energy level offsets as predicted by the freestanding layer calculation. The fact that subtle changes in structure can lead to energy offsets within a monolayer suggests an alternative means of tailoring energy alignment, e.g. by engineering lateral heterostructures.

Acknowledgments

We acknowledge financial support from the Austrian Science Fund (via project numbers S97-04, S97-14, P21330-N20 and P23190-N16), the Deutsche Forschungsgemeinschaft (project numbers TA-244/5-1/2 and KU-1531/2-1) and the EC 7th Framework Programme (grant number 226716). We also thank C Schüssler-Langeheine, M Ostler, T Seyller and the staff of BESSY II/Helmholtz-Zentrum Berlin for their support during the beamtime.

References

- [1] Kröger J, Jensen H, Berndt R, Rurali R and Lorente N 2007 *Chem. Phys. Lett.* **438** 249
- [2] Kilian L *et al* 2008 *Phys. Rev. Lett.* **100** 136103
- [3] Franke K J, Schulze G, Henningsen N, Fernández-Torrente I, Pascual J I, Zarwell S, Rück-Braun K, Cobian M and Lorente N 2008 *Phys. Rev. Lett.* **100** 036807
- [4] Soubatch S, Weiss C, Temirov R and Tautz F S 2009 *Phys. Rev. Lett.* **102** 177405
- [5] Koller G, Berkebile S, Oehzelt M, Puschnig P, Ambrosch-Draxl C, Netzer F P and Ramsey M G 2007 *Science* **317** 351
- [6] Puschnig P, Berkebile S, Fleming A J, Koller G, Emtsev K, Seyller T, Riley J D, Ambrosch-Draxl C, Netzer F P and Ramsey M G 2009 *Science* **326** 702
- [7] Puschnig P, Reinisch E M, Ules T, Koller G, Soubatch S, Ostler M, Romaner L, Tautz F S, Ambrosch-Draxl C and Ramsey M G 2011 *Phys. Rev. B* **84** 235427
- [8] Stadtmüller B *et al* 2012 *Europhys. Lett.* **100** 26008

- [9] Wießner M, Hauschild D, Schöll A, Feyer V, Winkler K, Krömker B and Reinert F 2012 *Phys. Rev. B* **86** 045417
- [10] Kraft A, Temirov R, Henze S K M, Soubatch S, Rohlfing M and Tautz F S 2006 *Phys. Rev. B* **74** 041402
- [11] Schull G and Berndt R 2007 *Phys. Rev. Lett.* **99** 226105
- [12] Fernández-Torrente I, Franke K J and Pascual J I 2008 *J. Phys.: Condens. Matter* **20** 184001
- [13] Seidel C, Awater C, Liu X D, Ellerbrake R and Fuchs H 1997 *Surf. Sci.* **371** 123
- [14] Seidel C, Poppensieker J and Fuchs H 1998 *Surf. Sci.* **408** 223
- [15] Zou Y, Kilian L, Schöll A, Schmidt T, Fink R and Umbach E 2006 *Surf. Sci.* **600** 1240
- [16] Broekmann L, Tadich A, Huwald E, Riley J, Leckey R, Seyller T, Emtsev K and Ley L 2005 *J. Electron Spectrosc. Relat. Phenom.* **144–147** 1001
- [17] Perdew J P, Burke K and Ernzerhof M 1996 *Phys. Rev. Lett.* **77** 3865
- [18] Gonze X *et al* 2009 *Comput. Phys. Commun.* **180** 2582
- [19] Kresse G and Hafner J 1993 *Phys. Rev. B* **47** 558
- [20] Kresse G and Joubert D 1999 *Phys. Rev. B* **59** 1758
- [21] Blöchl P E 1994 *Phys. Rev. B* **50** 17953
- [22] Grimme S 2006 *J. Comput. Chem.* **27** 1787
- [23] Glöckler K, Seidel C, Soukopp A, Sokolowski M, Umbach E, Böhringer M, Berndt R and Schneider W D 1998 *Surf. Sci.* **405** 1
- [24] Böhringer M, Schneider W D, Glöckler K, Umbach E and Berndt R 1998 *Surf. Sci.* **419** L95
- [25] Braun D, Schirmeisen A and Fuchs H 2005 *Surf. Sci.* **575** 3
- [26] Mercurio G *et al* 2013 *Phys. Rev. B* **87** 045421
- [27] Ziroff J, Forster F, Schöll A, Puschnig P and Reinert F 2010 *Phys. Rev. Lett.* **104** 233004
- [28] Rohlfing M, Temirov R and Tautz F S 2007 *Phys. Rev. B* **76** 115421
- [29] Garcia-Lastra J M, Rostgaard C, Rubio A and Thygesen K S 2009 *Phys. Rev. B* **80** 245427